# Preparation of Ultrathin and Degradable Polymeric Films by Electropolymerization of 3-Amino-L-Tyrosine

*Tommaso Marchesi D'Alvise[1], Sruthi Sunder[1], Roger Hasler[2], Julia Moser[1], Wolfgang Knoll[2], Christopher V. Synatschke[1], Sean Harvey[1]* and Tanja Weil[1]**

1 Max Planck Institute for Polymer Research, Ackermannweg 10, 55128 Mainz, Germany

2 Austrian Institute of Technology GmbH, Biosensor Technologies, Konrad-Lorentz-Strasse 24, 3430 Tulln, Austria

E-mail: Sdharv@gmail.com, weil@mpip-mainz.mpg.de

KEYWORDS Bioinspired bioderived polymeric films, electrodeposition, green polymer chemistry, polynorepinephrine, poly-aminotyrosine, biodegradable polymeric films

ABSTRACT

The resource intensive and environmentally unfriendly synthesis, recycling, and disposal of today's plastics has sparked interest in greener polymer processing. Bioderived polymers are one of many current areas of research that show promise for a sustainable future. One bioderived polymer that has been in the spotlight for the past decade due to its unique properties is polydopamine (PDA). Its ability to adhere to virtually any surface showing high stability in a wide pH range from 2-10 and in several organic solvents makes it a suitable candidate for several applications ranging from medical devices, coatings to biosensing applications. However, its strong and broad light absorption limits many applications that rely on transparent material, moreover fluorescence applications are limited by the high quenching efficiency of PDA. Therefore, new bioderived polymers that share similar features as PDA without fluorescent quenching are highly desirable. In this study, the electropolymerization of a bioderived analogue of dopamine, 3-amino-L-tyrosine (ALT) is demonstrated. The properties of the resultant polymer, poly-amino-L-tyrosine (p-ALT), exhibit several characteristics complementary to or even exceeding those of PDA and of its analog, poly-norepinephrine (p-NorEp), rendering p-ALT attractive for the development of sensors and photoactive devices. Cyclic voltammetry, spectroelectrochemistry and electrochemical quartz crystal microbalance have been applied to study the electrodeposition of this material and the resulting polymeric films have been compared to PDA and p-NorEp. Impedance spectroscopy revealed increased ions permeability of p-ALT with respect to PDA and p-NorEp. Moreover reduced fluorescence quenching of p-ALT film was achieved supporting its application as coating for biosensors, organic semiconductors and new nanocomposite materials.

## INTRODUCTION

The great demand of our society for more environmentally friendly and green processes has inspired new research into bioderived polymeric materials. Extraction and processing of large, complex biopolymers such as cellulose, chitin and carbohydrates for industrial usage have been developed during the past decades but they often require large quantities of hazardous chemicals and produce extensive amounts of waste. Nowadays, small bioderived molecules as raw material have attracted broad attention for bottom-up polymer synthesis as material properties can be controlled without waste production.[1,2] Although compounds such as terpenes and furans derived from biostocks have already shown great promise for the synthesis of commodity plastics such as poly(ethylene terephthalate) (PET) and polyethylene (PE), there is growing interest in new bioderived and biodegradable polymeric materials for specialty applications.[1,2,3] Phenol- and catechol-based derivatives are ubiquitous in Nature and they can be polymerized into functional materials or modified to generate new monomers for polymerization.[4–6] In this context, the amino acid L-tyrosine also serves as a precursor for many natural products.[7,8] For instance, dopamine, a neurotransmitter derived from L-tyrosine, has received much interest as a monomer for bioinspired polymer synthesis.[9,10] Dopamine is a major component of the mussel's byssus taking part in its unique ability to adhere to wet rocks.[11] Polydopamine (PDA) reveals similar properties and in the recent years, it has been under intensive investigations since it can be easily produced by self-oxidative polymerization in alkaline conditions.[11] It adheres to almost every surface showing high stability in a wide pH range from pH 2-10 and in many organic solvents. Such properties have made PDA a suitable candidate for several applications ranging from medical devices coating[12], to biosensing or membrane coatings for tailoring the surface properties of the target substrate.[13,14] Besides oxidative polymerization, PDA may also be achieved by electrochemical methods, such as cyclic voltammetry (CV), where a potential is swiped between two different values for several cycles.[15,16] In comparison to self-polymerization, the electrodeposition of dopamine proceeds faster, also in acidic solution, and affords more homogeneous films. Therefore, this method is very useful for coating different conductive substrates for a wide range of applications[9,17,18]. Electropolymerization has become a method of choice for the green synthesis and precise control of polymeric materials. In the meanwhile, also other bioderived monomers with similar chemical chemical structures as dopamine have been polymerized following this approach. The formation

of ultrathin films on conductive substrates, such as gold, as an additional layer providing surface groups for further functionalization is of emerging interest for generating biosensors, organic semiconductors and new nanocomposite materials.[9,19-21]

Herein, we report the electropolymerization of 3-amino-L-tyrosine (ALT) to generate poly-amino-L-tyrosine (p-ALT). For comparison, PDA and the structurally similar polymeric material poly-norepinephrine (p-NorEp)[22], were also prepared and characterized. p-NorEp is formed by polymerization of norepinephrine (NorEp) and shares similar adhesive properties as PDA, but with the advantage of higher hydrophilicity due to the additional aliphatic hydroxyl group of NorEp. This group also allows straight-forward post-functionalization, which is challenging to obtain with polydopamine coatings.[22] Until now, most studies on the electrodeposition of NorEp required pre-oxidation steps[23,24], which renders this polymerization more complicated limiting the advantages of the electropolymerization.[25,26] ALT is a synthetic derivative of L-tyrosine that may be enzymatically synthesized via a nitrotyrosine intermediate by reduction of the nitro group as depicted in Figure 1.[27] It has been used in the biosynthesis of the thermally sensitive chemiluminescent polymer diazo-luminomelanine used in microwave dosimetry research, which has also been copolymerized with dopamine to improve the electronic features of PDA.[28,29] In this study, the electropolymerization of p-ALT affords ultrathin p-ALT coatings, whose thickness can be controlled at the low nanometer scale. p-ALT offers several unique features such as very high surface smoothness and low fluorescence quenching, which clearly differentiate this polymeric material from electropolymerized PDA and p-NorEp. Therefore, p-ALT films could be of great interest for the development of sensors and photoactive devices. Moreover, we demonstrate that p-ALT is readily degraded by hydrogen peroxide. Finally, another advantage of electropolymerization is the complete green synthesis of these bioderived compounds which is possible to achieve by coupling it with a solar power generator as already advised by the scientific community.[30]

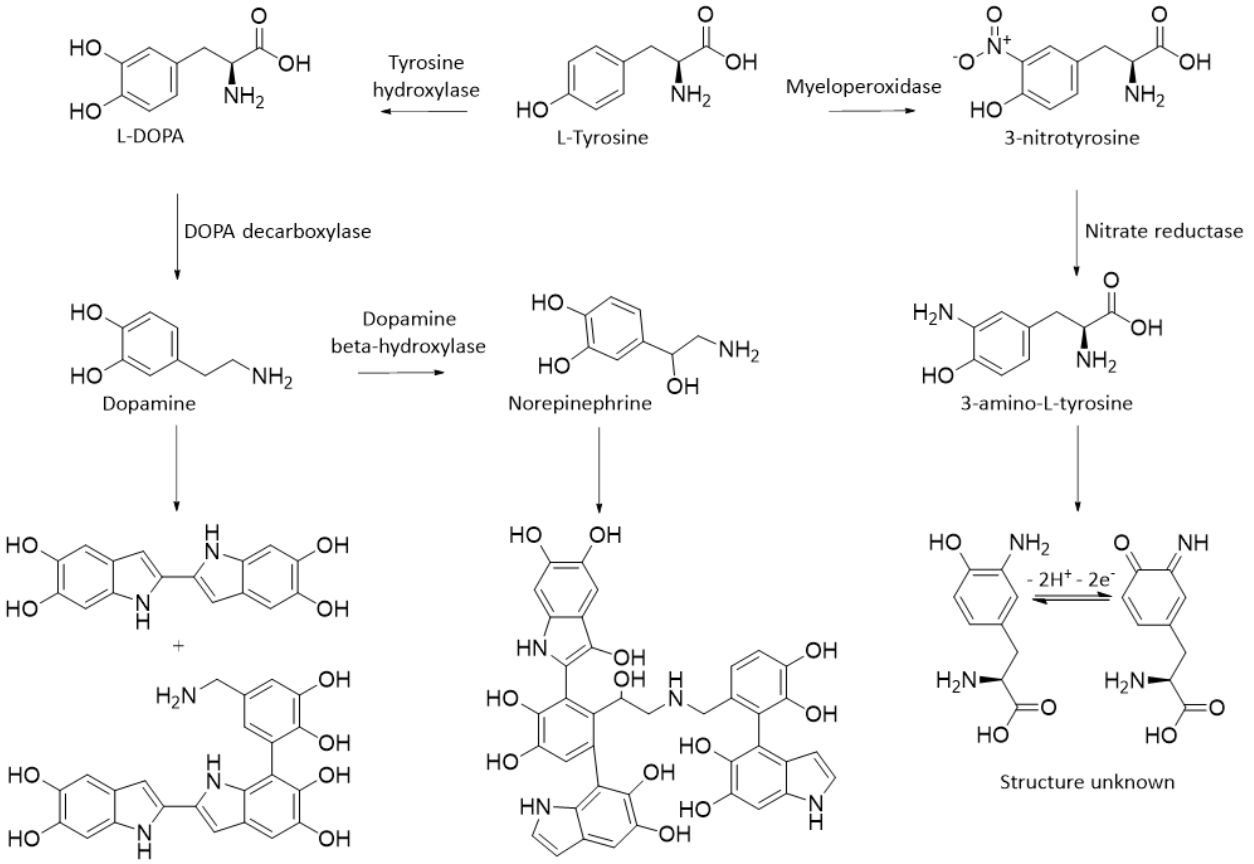


*Figure 1: Biosynthetic pathways for norepinephrine and 3-aminotyrosine. Relevant intermediates and catalytic enzymes are also given. Possible oligomeric structures arising from the polymerization of dopamine and norepinephrine as reported by Bisaglia et al* [31] *and Hong et al.* [32]*, respectively.*

## Materials and Methods

Gold coated (1000 Å) microscope slides (Sigma-Aldrich) were cut using a diamond tip. Phosphate buffer (pH 7, 100 mM), was prepared, using sodium phosphate dibasic anhydrous (99%) and sodium phosphate monobasic (99%) (Sigma-Aldrich) in Milli-Q water. Carbonate buffer (pH 10, 100 mM) was prepared, using sodium bicarbonate (>99.7%) and sodium carbonate (>99.8%) from Sigma-Aldrich, in Milli-Q water. Gold-coated quartz crystals (6 MHz) (Metrohm) were used for electrochemical quartz crystal microbalance measurements. Potassium ferricyanide (99+%) and potassium ferrocyanide trihydrate (99+%) were obtained from Acros Organics. Sodium dihydrogen phosphate was obtained from Sigma Aldrich and potassium hydrogen phosphate from Appli Chem.

Electropolymerization of the polymeric films

According to our previous work[33] electropolymerization and cyclic voltammetry experiments were performed using a Metrohm Autolab N series potentiostat (AUTOLAB PGSTAT 204) with a standard three electrode configuration. A gold covered glass microscope slide was used as the working electrode, Ag/AgCl, 3M KCl as the reference electrode, and a gold wire as the counter electrode for film preparation, while a platinum wire was used as counter electrode for electrochemical impedance spectroscopy experiments. All reactions were performed in a 35 mL electrochemical cell (Metrohm), under air atmosphere and at room temperature. Pre-treatment of the gold working electrode was performed by Ar plasma cleaning for 10 minutes at 6 mbar pressure. Gold was used as a substrate for electrodeposition of films due to its inertness, excellent conductivity, and low surface roughness.

Electropolymerization of polydopamine (PDA) films

The gold substrate was immersed in a solution of dopamine hydrochloride (1 mg/mL) dissolved in 100 mM phosphate buffer at pH 7.0. A potential was applied and cycled from +500 mV to -500 mV with a scan rate of 0.01 V/s to induce dopamine polymerization at the interface.

Electropolymerization of poly-norepinephrine (p-NorEp) films

The gold substrate was immersed in a solution of norepinephrine (1 mg/mL) dissolved in 100 mM phosphate buffer at pH 7.0. A potential was applied and cycled from +500 mV to -500 mV with a scan rate of 0.01 V/s to induce norepinephrine polymerization at the interface.

Electropolymerization of poly-aminotyrosine (p-ALT) films

The gold substrate was immersed in a solution of 3-aminotyrosine (1 mg/mL) dissolved in 100 mM phosphate buffer at pH 7.0. A potential was applied and cycled from +1200 mV to -500 mV with a scan rate of 0.01 V/s to induce 3-aminotyrosine polymerization at the interface.

Electrochemical quartz microbalance (EQCM) characterization of the polymer films

Electrochemical quartz microbalance was conducted in a 3 mL electrochemical cell using Ag/AgCl reference electrode and gold counter electrode, by minimizing the driving force prior starting the measurement.

Spectroelectrochemistry

All reactions were performed in a standard quartz cuvette electrochemical cell placed in a cuvette holder ported for fiber optic connectors on three sides. Same as above, a 3-electrode setup was used with a gold coated microscope slide as working electrode, a gold wire as counter electrode and Ag/AgCl reference electrode. In addition, the light from a deuterium and halogen lamp was passed through the reaction solution directly in front of the working electrode via fiber optic connection and the transmitted light collected by a spectrophotometer. The electropolymerization was performed under air atmosphere and at room temperature. Pre-treatment of the gold working electrode was performed by 10 minutes in Ar plasma cleaning at pressure of 6 mbar. The same procedure described above was used for each respective monomer. Absorbance was calculated using the initial spectrum for each solution (immediately before beginning electropolymerization) as reference.

Electrochemical Impedance Spectroscopy (EIS)

Electrochemical impedance spectroscopy was conducted on 1 $cm^2$ coated electrode surface using a 5 mM solution of equimolar $K_3[Fe(CN)_6]/K_4[Fe(CN)_6]$ in phosphate buffer (pH 7, 100 mM 1.5 mL) confining the analyzed area with an O-ring of 8 mm in diameter. As a counter electrode a Pt wire was used, the applied potential was 0.2 V against Ag/AgCl reference electrode with an amplitude of 0.01 V and applying a frequency from 0.01 to $10^5$ Hz. The data were fitted and analyzed using the software Nova 2.1.

Atomic Force Microscopy (AFM)

Atomic force microscopy was used to physically characterize the film, measure the morphology, surface roughness and thickness of the polymer films on gold by scratching it with a plastic tip after it was freshly prepared. The profile of the scratch was then recorded by AFM (Park NX20) with a cantilever 70 KHz resonance frequency and an elastic constant of 2 N/m.

Fourier Transform Infrared Spectroscopy (FTIR)

The infrared spectrum of the film on gold obtained by grazing-angle reflectance FTIR (Vertex 70, Bruker) after purging the sample with dry air for 15 minutes and recording 4 spectra at 3000 scans with an interval of 1 minute between each one.

X-ray Photoelectron Spectroscopy (XPS)

XPS was conducted using a Kratos Axis UltraDLD spectrometer 3 (Kratos, Manchester, England) using an Al K excitation source with a photon energy of 1487eV. The data was acquired in the hybrid mode using a 0° take-off angle, defined as the angle between the surface normal and the axis of the analyzer lens. Detailed region XP spectra were collected with setting analyzer pass energy at 80 eV, and a linear background was subtracted for all peak quantifications. The peak areas were normalized by the manufacturer supplied sensitivity factors and surface concentrations were calculated using CasaXPS software. N 1s, C 1s and O 1s high-resolution spectra were collected with analyzer pass energy of 20 eV. A Neutralizer was always used during spectra collection.

Surface Plasmon Resonance (SPR) experiments

*Fabrication of gold-coated optical fiber substrates*

Plasmonic fiber optic (FO) probes were prepared according to previously reported procedures.[34] Tips of 6.5 cm in length were cut from TECS-clad multimode optical fiber cable (Thorlabs) with a numeric aperture of 0.39 and a core diameter of 1000 µm. At one end of the tip an optically active section for surface plasmon resonance (SPR) was constructed by removing the outer jacket layer with a dedicated mechanical stripping tool and subsequent dissolution of the inner polymer cladding with acetone. Obtained tips were cleaned with Milli-Q water, *iso*propanol and blow dried with compressed air before coating them homogenously with 50 nm of gold in an EM ACE600 sputter coater (Leica Microsystems) using a sputter rate of 0.11 nm/s on a rotating stage. As-sputtered FO tips were further thermally annealed at 180°C for 7 h according to a previously reported procedure.[35] As reported, mild thermal treatment results in a morphological change associated with a grain growth of the vacuum-deposited gold layer. This ensured a better stability

of the Au film during the electropolymerization step and blue-shifted the plasmonic signal, leading to a larger operational window for polymer films with a higher refractive index. To ensure a good electrical connection across the transition of the upper gold-coated part of the fiber to the thinner optical active section, conductive silver paint (Ag-paint, RS Components Ltd) was applied and dried at room temperature for 2 h. To avoid a possible influence of the silver coating, this section was further coated by applying a liquid heat shrink tubing (Performix Liquid Tape, Plastidip®, Plasti Dip Europe GmbH) and dried at room temperature for 16 h. As-prepared FO probes were stored under Argon until further usage.

*Optic fiber (FO)-SPR measurements*

FO probes were connected to a Y-optical splitter (400 µm core diameter, numeric aperture of 0.39, Thorlabs) with a commercially available bare fiber terminator (Thorlabs) via a SMA905 connection. Polychromatic light (Quartz Tungsten-Halogen lamp, 400-2200 nm, 50 mW, Thorlabs) was focused with an achromatic lens (Thorlabs) on the backend of an input arm of the Y-optical splitter and guided to the tip of the plasmonic fiber probe in order to resonantly excite propagating surface plasmons on its lateral gold surface. The light is back reflected at the gold-coated cross section of the tip and collected in a spectrometer (HR4000CG-UV-NIR, OceanOptics Inc.), connected to the output arm of the Y-optical splitter. The measured back reflected spectrum was normalized with that of the tip in air. In case of p-ALT coated fiber tips, a reference spectra of a gold-coated FO tip in air (without polymer layer) was used, because the high refractive index of p-ALT would lead to a plasmonic feature in the detectable range of the reference spectra recorded in air. FO probes were then dipped into Milli-Q water and normalized reflectivity spectra were recorded. The acquisition time of the spectrometer was set to 5 ms and 100 spectra were averaged per measurement point. The minimum position of the plasmonic dip (resonance wavelength $\lambda_{SPR}$) in the normalized reflectivity spectra was fitted and tracked over time using a dedicated LabVIEW software.[36]

Fluorescence studies

A polydimethylsiloxane (PDMS) mask with a 3 mm diameter hole was placed on the surface of each film. 10 µL of a 1 mg/ml solution of Fluorescein Isothiocyanate (FITC) in 100 mM phosphate

buffer (pH 8.5) was introduced into the hole and incubated overnight. The next day, each film was washed with phosphate buffer (pH 7.0) and Milli-Q water, then incubated for 72 hours in a pure phosphate buffer (pH 7.0) to remove unbound FITC. A new phosphate buffer (pH 7.0) was added to the films and they were imaged on an epi-fluorescence microscope using a FITC filter set. A 10x objective was used.

Degradation studies

Oxidative degradation of the polymeric films in $H_2O_2$ was investigated by incubating the films for 4 intervals of 22 h and one interval of 3 days in 9 mL of a 50 mM solution of $H_2O_2$ in Milli-Q water at room temperature for several days. The degree of degradation was investigated by AFM, by measuring the changes in the depth profile at every interval and by cyclic voltammetry of $K_3[Fe(CN)_6]/K_4[Fe(CN)_6]$ before and after the degradation experiment.

**Results and Discussions**

The p-ALT thin films were prepared by electropolymerization using cyclic voltammetry and compared to PDA and p-NorEp films that have both very similar cyclic voltammograms. For PDA and p-NorEp, the upper and lower vertex potential used were +0.5 V and –0.5 V, respectively (Figure 2A, B). In both cyclic voltammograms, an oxidation peak at +0.3 V due to the oxidation of catechol to quinone is observed during the first electrochemical cycle. A reduction peak for the reverse reaction, quinone to catechol, appears at –0.3 V for PDA and -0.2 V for p-NorEp. In both cases, the current decreases over each electropolymerization cycle due to the deposition of an insulating polymer layer, which occurs until the tenth cycle, when oxidation and reduction peaks are no longer distinguishable. Despite the similarities in the chemical structure of dopamine, NorEp and ALT, the electropolymerization of ALT proceeds markedly different. Cyclic voltammetry of ALT using an upper vertex of +0.5 V revealed an oxidation peak around +0.3 V (Figure S1) but did not yield a robust film. Previous efforts to electropolymerize 2-aminophenol, a structurally similar molecule, also reported no film formation at lower potentials but instead required potentials as high as +1.2 V.[37–39] A second oxidation peak could then be observed around +0.8V, which was attributed to the oxidation of the aromatic amino group (Figure S3). Therefore, the upper vertex for ALT was also increased to +1.2 V, while the lower vertex potential was kept at −0.5 V in order to facilitate oxidation of the amino group leading to more efficient film

formation. In the cyclic voltammogram of ALT presented in Figure 2 C, a sharp phenol oxidation peak is observed at +0.3 V and a second oxidation peak occurs at +0.8 V, likely due to the oxidation of the amine present at the aromatic ring. In contrast to PDA and p-NorEp, less reduction in the current is observed after each cycle indicating the formation of a less insulating layer.

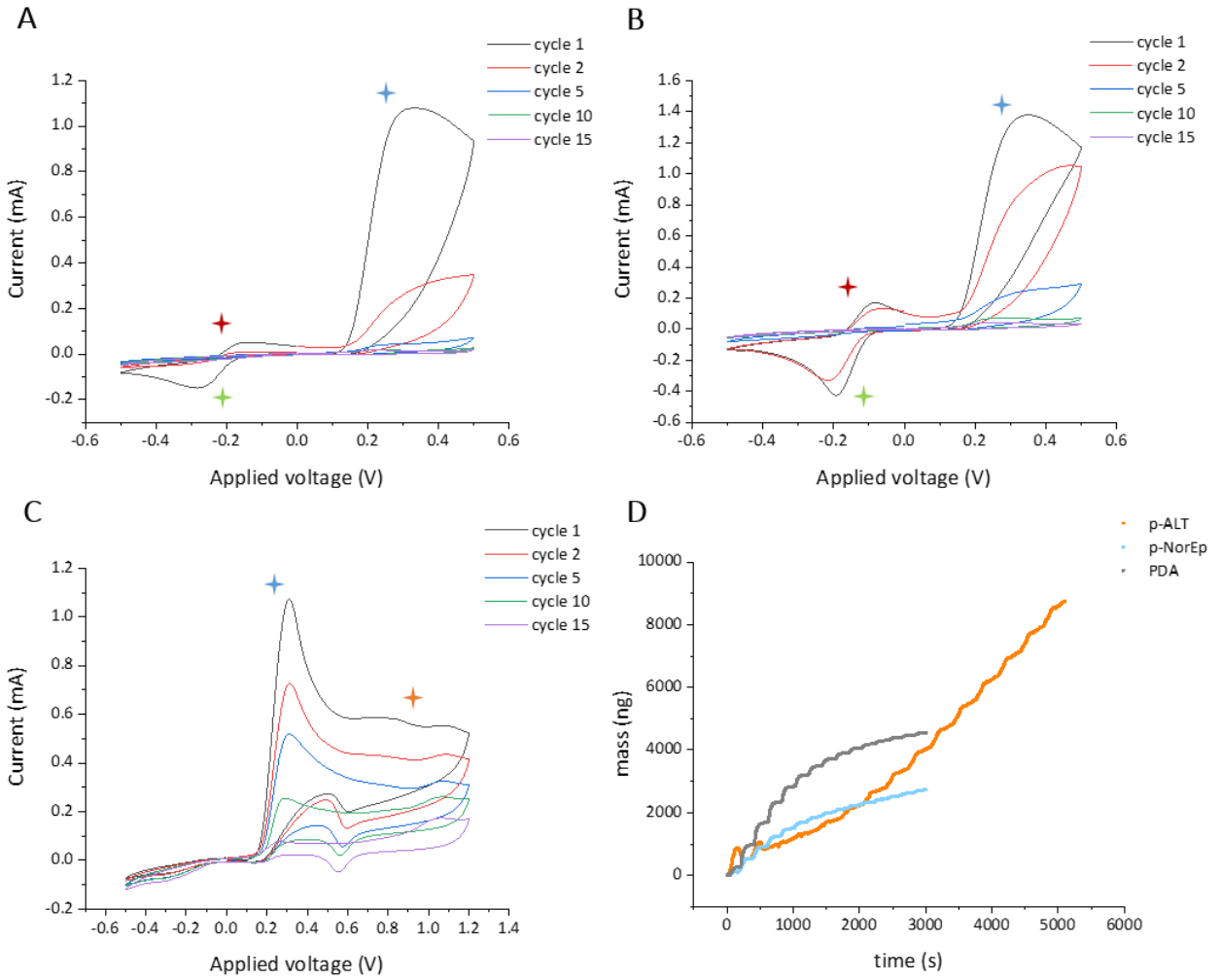


*Figure 2: Cyclic voltammetry (A,B,C) and electrochemical-QCM data (D). A. PDA cyclic voltammetry shows a first oxidation peak at +0.3V attributed to the oxidation of catechol to quinone (blue star), a reduction peak (green star) and an oxidation peak (red star), attributed to the redox activity of leucodopaminechrome. B. p-NorEp cyclic voltammetry reveals a first oxidation peak at +0.3V attributed to the oxidation of the catechol to quinone (blue star), a reduction peak (green star) and an oxidation peak (red star) attributed to the redox activity of aminochrome structures and benzaldehydes that are shown at –0.2V and –0.1V, respectively. C. p-ALT cyclic voltammogram with oxidation peaks from the aromatic hydroxyl group (blue star) and amino group (orange star) at +0.3 V and +0.9 V, respectively. The current decreases rapidly with each cycle for PDA and pNorEp due to the formation of an insulating polymeric film. p-ALT exhibits a smaller decrease in current suggesting the formation of a less insulating film. D. EQCM mass deposition over time is represented indicating an asymptotic deposition behavior from PDA and p-NorEp, while p-ALT reveals and unusual increase in the film deposition rate.*

Mass deposition during the electropolymerization of all three monomers was tracked using eQCM. By monitoring the oscillation frequency of a gold-coated quartz crystal used as a working electrode, the deposition of the polymer at the electrode is observed as a decrease in the frequency of the crystal. For PDA and p-NorEp, mass deposition is highest during the first four or five cycles and exhibits a continuous decrease in the deposition rate with further cycles, reaching an asymptotic deposition rate over time (Figure 2D). This behavior matches well with the results from the cyclic voltammetry experiments, where the current decreases rapidly over the first five cycles with smaller changes thereafter. Together, these data indicate an early, rapid deposition of insulating PDA or p-NorEp oligomeric layers with the reduction in current on further cycling limiting the later deposition. This observation is in line with previous reports that the electropolymerization of dopamine exhibits a self-limiting thickness.[16] Interestingly, for p-ALT, the deposition rate increases after the first three cycles and even after the 14$^{th}$ cycle, suggesting the formation of a much less insulating film compared to PDA and p-NorEp, as shown in Figure 2D. The structure of polycatecholamines have not been fully elucidated yet and the formed polymeric structures are likely affected by i.e. the oxidation agent, buffer solution and temperature at which the oxidative polymerization takes place.[40] These highly crosslinked polymeric materials are most likely composed of a complex mixture consisting of low order oligomers of indole units held together by supramolecular interactions (Figure S2).[41] In PDA and p-NorEp, the long-range conjugated system is disrupted, which is responsible for their insulating or semi-conductive characteristics. Until now no film formation and no chemical structures have been reported for p-ALT. However, polymers based on 2-aminophenol have been analyzed and phenoxazine ladder structures were proved responsible for the conductive features (Figure S4).[37,38,42] Similar to 2-aminophenol, p-ALT films provide increased conductivity compared to other polycatecholamines, which could be due to indole oligomerization and phenoxazine structure formation. The eQCM frequency changes with the number cycles and density of the deposited films can be derived using the Sauerbry equation (eq. 1), where $\Delta f$ is the frequency change due to mass deposition and $C_f$ is a characteristic constant of the quartz crystal electrode. In combination with the thickness measured by AFM, an estimation of the material density can be calculated since the Sauerbry equation used for the eQCM mass estimation assumes a uniform and compact film.[43] The results are listed in table 1.

$$-\Delta f = \Delta m \cdot C_f \qquad C_f = 0.0815 \frac{H_z}{ng}/cm^2 \quad (1)$$

*Table 1: Density of the films calculated through equation 1.*

| | Density (g/cm$^3$) | | |
|---|---|---|---|
| | 5 cycles | 10 cycles | 15 cycles |
| PDA | 1.79 | 1.91 | 1.75 |
| p-NorEp | 1.66 | 1.43 | 1.41 |
| p-ALT | 1.43 | 1.52 | 1.38 |

Unexpectedly high film densities[44] were obtained (Table 1), which were highest in PDA. These high densities could be attributed to the electrochemical deposition process leading to the formation of a particularly dense and homogeneous film, as previously discussed in literature[45]. For all polymeric films prepared, the densities decrease after 15 cycles, possibly due to the deposition of a less well packed material. This observation is more evident in the case of p-ALT, where a density drop to 1.38 g/cm$^3$ was observed. For p-NorEp, the density values decreased from the fifth to the tenth cycle while remaining almost constant thereafter. It is also worth to consider that the assumptions at the base of the Sauerbry equation can lead to an overestimation of the film density, although the relative comparison between the different films remains valid. The thicknesses and morphologies of the deposited films were studied using AFM. In Figure 3, the micrographs obtained from PDA, p-NorEp and p-ALT after ten electropolymerization cycles are shown. Overall, the films appear smooth and homogeneous. PDA and p-NorEp show some nodules higher than 30 nm and the number of nodules increases for higher numbers of electropolymerization cycles, suggesting multiple deposition mechanisms. Although some nodules are present, p-NorEp appears to be comparatively smoother than PDA. On the other hand, p-ALT almost completely lacks nodules, indicating a uniform deposition mechanism. The film thickness

for p-NorEp and for PDA increases almost linearly from 8.5 nm to 17 nm with increasing cycles. In contrast, the thickness of p-ALT films increases from 11 nm to 46 nm (Figure 3D) reaching a value three times higher than the other two films. These results are in line with eQCM data supporting the insulating behavior of p-NorEp and the less insulating features of p-ALT. The surface roughness of both p-NorEp and p-ALT exhibits a slight thickness-dependent increase, but it is still close to that of the gold electrode and considerably lower than PDA.

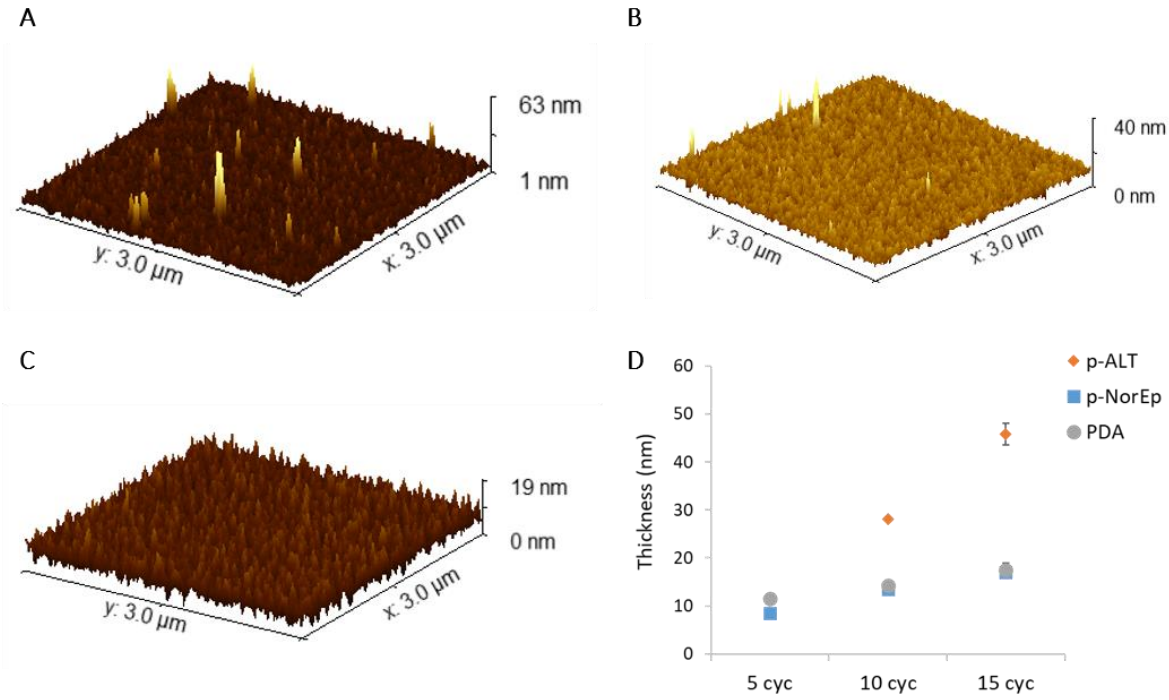


*Figure 3:A, B and C. AFM micrograph of ten cycles electrodeposited films on gold of PDA p-NorEp and p-ALT, respectively. D. thickness dependence on the number of cycles for the three different polymeric films.*

To gain more information on the chemical structure of the resultant p-ALT, PDA and p-NorEp films, x-ray photoelectron spectroscopy (XPS) was performed. XPS signatures from C, N and O were obtained from high resolution spectra for all films after ten cycles of electrochemical deposition[46,47] (Figure S5). The area percentages indicating the abundance of the different functional groups in the films are summarized in Table 2. PDA and p-NorEp show similar percentage values for C1s spectra indicating similarity in the final polymeric structure. Compared to PDA, p-NorEp reveals a similar distribution in the amine and amide groups but a higher content of hydroxyl groups, most likely due to the additional aliphatic hydroxyl group of NorEp. On the

other hand, p-ALT reveals a much higher percentage corresponding to the carbonyl group, possibly originating from condensed carboxylic acid products in p-ALT molecule.

*Table 2: Area percentage of the different functional group contributions in the high-resolution XPS spectra.*

| | | PDA | p-NorEp | p-ALT |
|---|---|---|---|---|
| C1s | C-C % | 44.3 | 41.6 | 40.1 |
| | C-OH % | 46.5 | 47.9 | 43.8 |
| | C=O % | 9.2 | 10.5 | 15.9 |
| O1s | C-OH % | 54 | 78.6 | 76.3 |
| | C=O % | 46 | 21.4 | 23.6 |
| N1s | $R_2$-NH % | 52.3 | 50.9 | 37.6 |
| | R-$NH_2$ % | 28.3 | 33.7 | 17.8 |
| | RN= % | 19.4 | 15.4 | 44.5 |

Next, changes in the composition of the soluble fraction of intermediates formed during electropolymerization were investigated using in-situ UV-Vis spectroscopy. p-NorEp and PDA exhibit similar spectra changes over the course of the electropolymerization process (Figure 4). Initially, peaks around 300 nm and 480 nm are observed, similar to the autoxidation of catecholamines, due to the presence of aminochrome-like structures formed from the initial oxidation and cyclization of the cathecolamines.[31] Later, a continuous increase in the absorbance across the visible spectrum is seen due to further oligomeric and polymeric species.[31,48] The spectra

of p-ALT electropolymerization, on the other hand, indicate a different mechanism (Figure 4). The spectra are dominated by overlapping peaks centered at 340 nm, attributed to the conjugation of two ALT monomers, and at 430 nm, which have been attributed to the formation of phenoxazine structures in the oxidation of aminophenol.[49,50] Similar to poly(aminophenol) formation, phenoxazine structures could in principle serve as new monomers during the generation of p-ALT resulting in different polymeric structures compared to p-NorEp and PDA.[38,51,52]

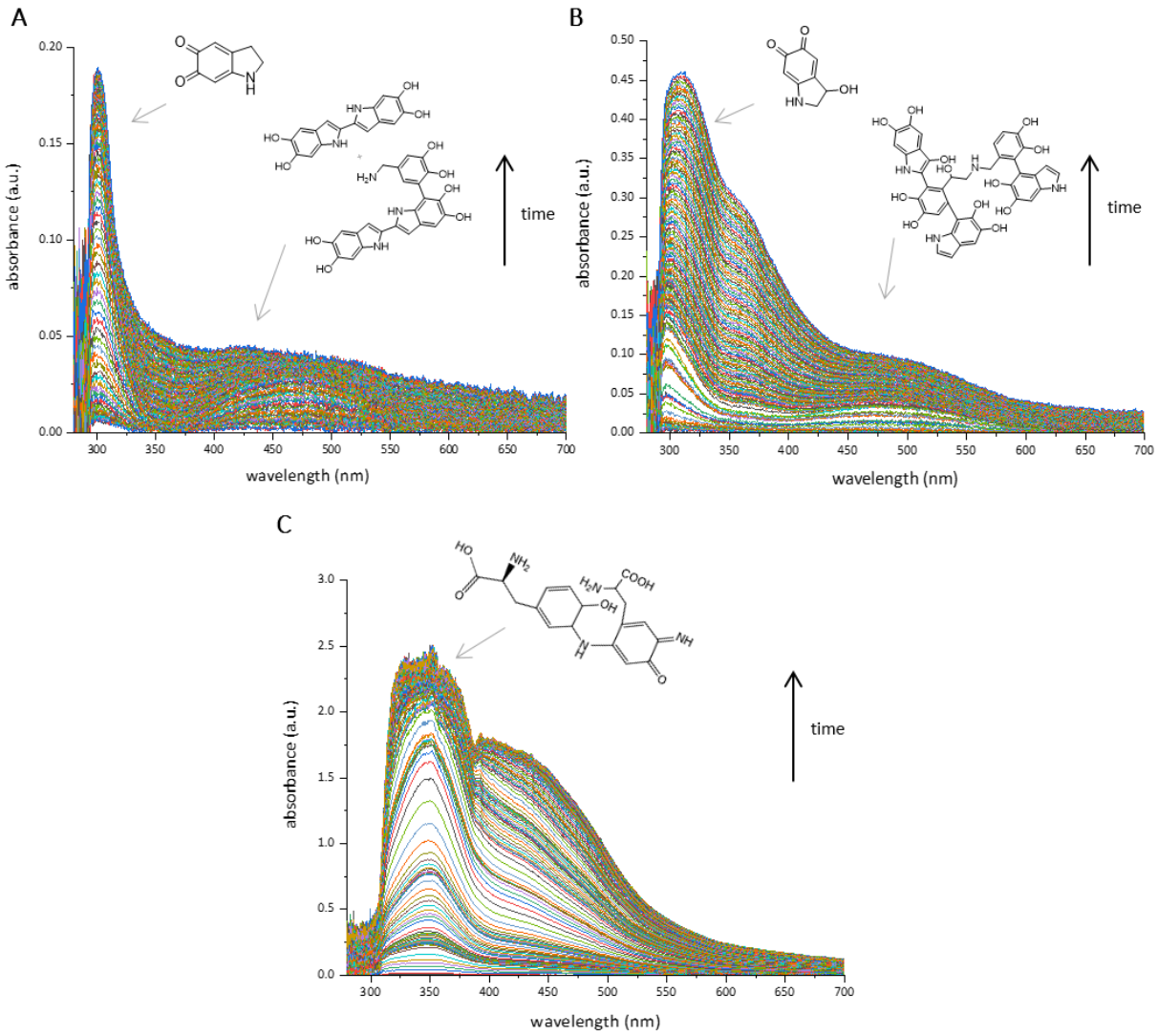


*Figure 4. In-situ UV-Vis absorbance for A. PDA, B. p-NorEp and C. p-ALT during 15 cycles of CV.*

In order to obtain a more comprehensive chemical analysis of the synthesized films, the FTIR spectra of all three polymer coatings have been recorded as depicted in Figure S7. All three films

show polymeric broad band absorbance around 3500 $cm^{-1}$ and at 1600 $cm^{-1}$ with few appreciable differences in the fingerprint region. Next, the electrodes with the coated films were characterized by electrochemical impedance spectroscopy (EIS), using a 5 mM solution of potassium ferrocyanide in phosphate buffer pH 7 as a redox probe in a frequency range between 0.01 and $10^5$ Hz. In EIS, the resistance to electron transfer is represented by the semicircle diameter in the Nyquist plot[53,54] (Figure 5). The gold surface with the deposited film was characterized for five and 15 cycles of deposition. The data were fitted with a Randle equivalent circuit formed by a resistance, attributed to the solution (Rs) in series, with a resistance and a constant phase element placed in parallel, in order to extract the resistance to charge transfer (Rct) as shown in Figure 5. In the case of PDA and p-NorEp, the samples could be fitted from 100 kHz to 0.01 Hz while for p-ALT this was not possible since the samples were probably undergoing changes during the measurements. For this reason, the fit of p-ALT samples was done considering the portion of data until 0.1 Hz where the material was mostly stable. In that region, the measurements conformed to the Kramer-Kronig test, which correlates the real and imaginary part of the spectrum as belonging to a system, which is linear, casual and invariant with time. The data are fitted with a sufficiently general model built as a resistor with a number (N) of RC elements in series to estimate the final validity. As expected, the resistance to charge transfer derived from the film increased rapidly with higher deposition cycles and film thickness as shown previously.[55,25] p-ALT exhibited the lowest resistance although formed the thickest films suggesting the formation of a less compact structure compared to PDA and p-NorEp, which supports the results of the density measurements. However, another explanation for these observations could be that the p-ALT film is permeable to ions. Over three consecutive measurements on the same sample, the resistance to charge transfer decreased in the high frequency range of the impedance spectrum. Contrary, in the low frequency region, the resistance is substituted by a straight line indicating a resistance to mass transfer, known as Warburg resistance. The observed phenomena would suggest that the p-ALT film is composed of a porous structure that can, overtime, absorb the electrolyte, allowing free movements of ions, thereby exhibiting reduced resistance. The behavior was studied in several samples and the values of Rct extracted from the fit are plotted in Figure S8. Moreover, the observation is in agreement with the different deposition rates depicted by EQCM experiments. Among the three poly-catecholamines studied, PDA shows the highest resistance when deposited with only five cycles

while p-NorEp reveals the same behavior as PDA after 15 cycles of deposition confirming the formation of a homogeneous and insulating polymer coating.

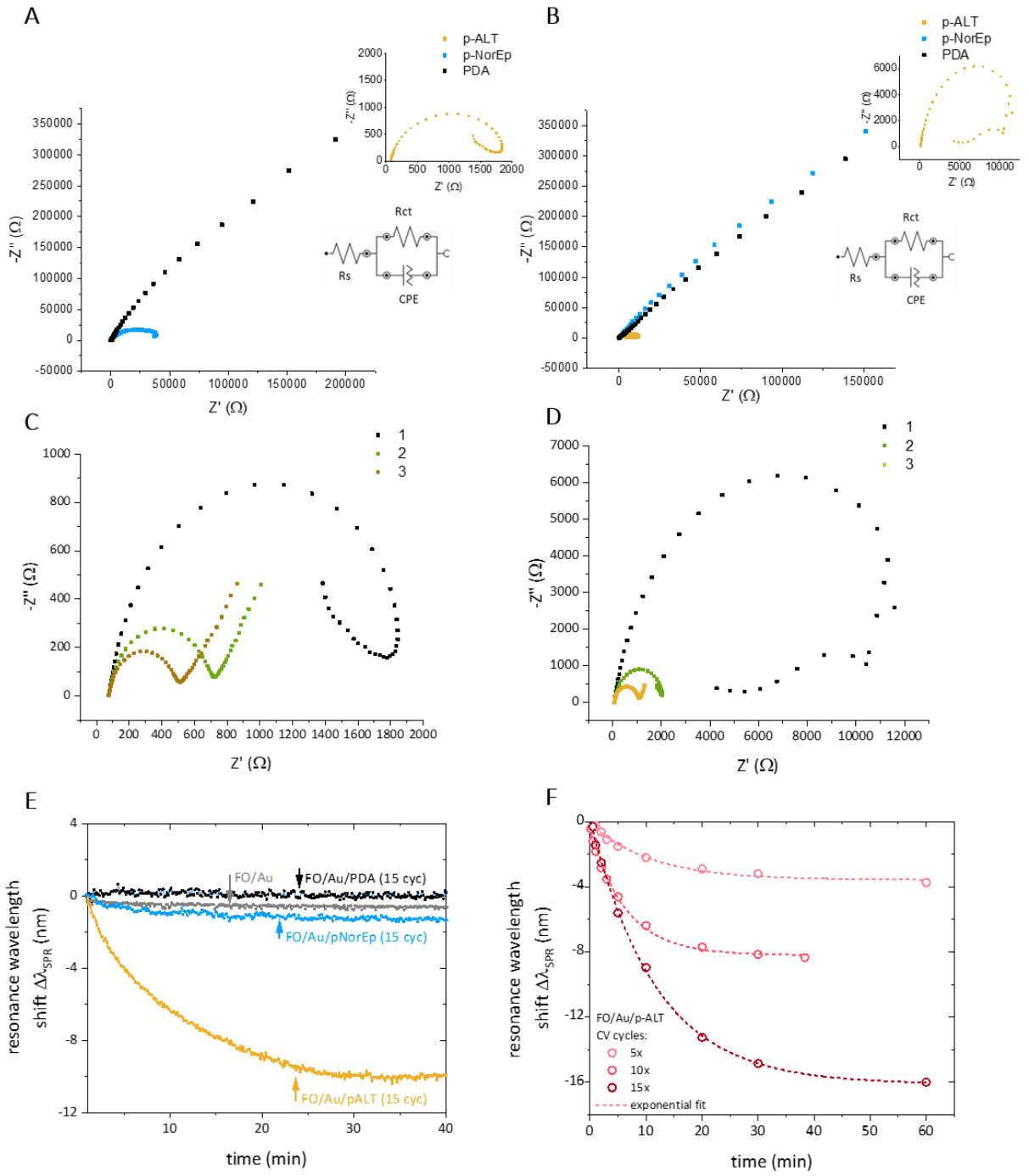


*Figure 5. Electrochemical Impedance Spectroscopy data for PDA, p-ALT, and p-NorEp. A. 5 cycles and B. 15 cycles. Inset: Magnification of the p-ALT region. C. Impedance spectroscopy of p-ALT 5 cycles and D. p-ALT 15 cycles with repetitively performed on the same samples to show the progressive decreasing of impedance over the three times repetitive measurements E.*

*Shift in wavelength of the resonance dip for the three different materials at the higher thickness. F. Resonance wavelength shift for the three different thicknesses of ALT film, showing an exponential decay.*

Due to the lower temporal resolution of the EIS measurements, in order to further investigate and monitor the apparent swelling phenomena of the films, a surface plasmon resonance (SPR) technique was employed to understand the change that the p-ALT matrix undergoes in solution. The shift originating from the resonance dip was monitored over time in order to prove the swelling behavior. The SPR signal shifted to lower wavelengths over time after immersion of the substrate in water (Figure 5E), which was attributed to the permeation of water into the matrix resulting in an increase of porosity and decrease of optical density. The shift was noticeable only for the p-ALT matrix while PDA and p-NorEp did not show significant changes over time, as shown in Figure 5E, as expected from the impedance measurements. More investigations were carried out comparing three film thicknesses for the p-ALT matrix (5, 10 and 15 cycles); the data clearly shows a drift attributed to swelling for all three different thicknesses. In addition, an increase of the drift signal proportional to the thickness of the sample is observed. The data could also be fitted with an exponential decay reaching steady state after 30, 40 and 60 minutes of immersion for 5, 10 and 15 cycles, respectively. Polycatecholamines such as PDA are known to be potent fluorescence quenchers[56–58] which makes them unsuitable for some applications where fluorescence is important, such as chromophore-based sensors and reporters.[59] The quenching behavior is attributed to the nanostructure of PDA possessing a high degree of π-π interactions.[59] Through the introduction of phenoxazine structural units, p-ALT is expected to have a different nanostructure to that of other polycatecholamines and thereby may have a lower degree of quenching. To determine the relative quenching effect, each film was incubated overnight with a 1 mg/ml solution of Fluorescein Isothiocyanate (FITC) solution in phosphate buffer pH 8.5, restrained to a 3 mm diameter area of the film using a PDMS mask (Figure S9). After washing and incubation in a pure phosphate buffer (pH 7.0) for 72 hours, the films were imaged on an epi-fluorescence microscope. It can be clearly observed that p-ALT exhibits a significantly higher fluorescence to that p-NorEp and PDA (Figure 6A, B, C) suggesting that it is a less potent quencher. Therefore, for applications using fluorescence for reporting, p-ALT is a better option than p-NorEp and PDA.

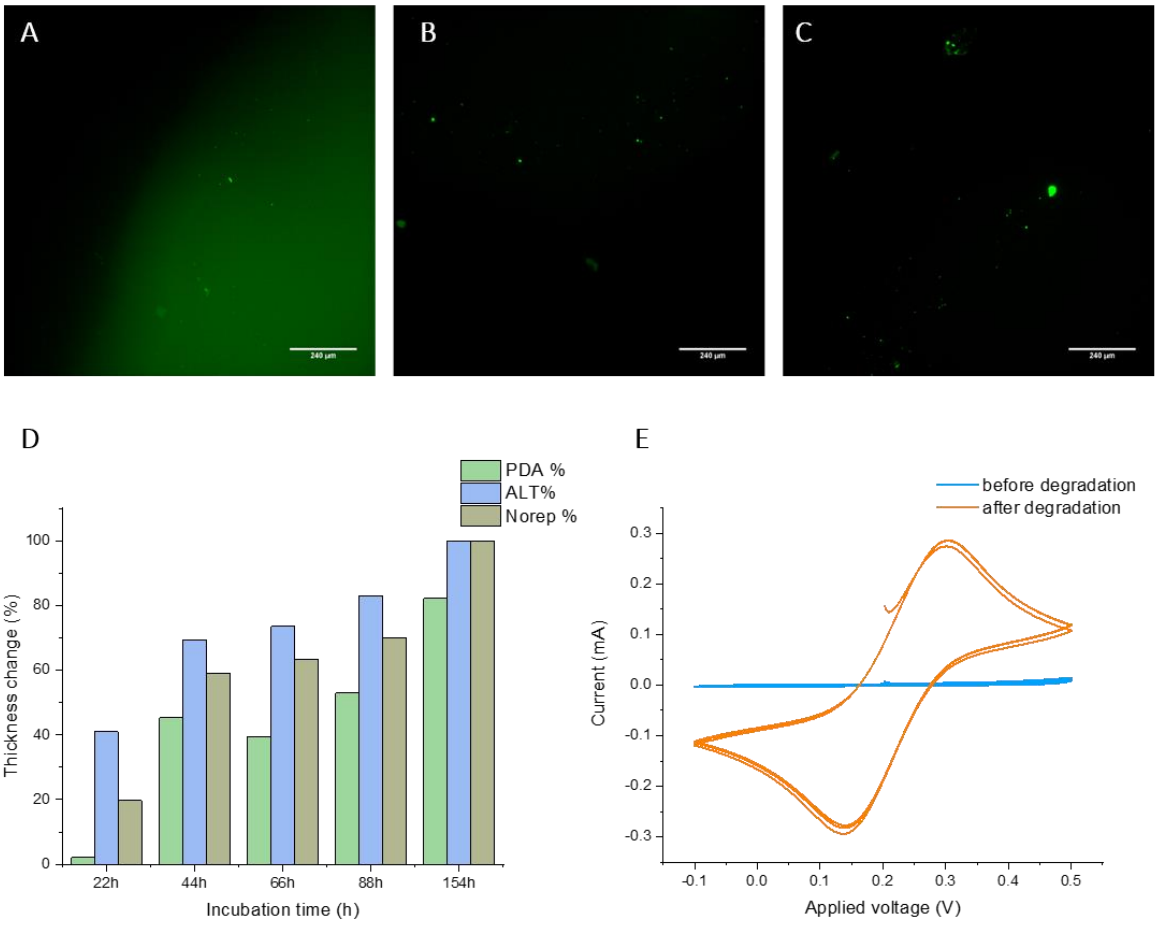


*Figure 6: Fluorescence images of p-ALT (A), p-NorEp (B) and PDA (C) after overnight incubation with 1 mg/ml FITC. Images were taken through a 10x objective using a FITC filter set. Scale bar = 240 µm. D. Thickness change in percentage for 5 cycle p-ALT, 10 p-NorEp and PDA after incubation in $H_2O_2$ 50 mM for 154 h D. Example of $K_3[Fe(CN)_6]/K_4[Fe(CN)_6]$ cv on PDA film before and after the degradation study.*

To evaluate the degradability of the films, the effect on the film integrity by the incubation in 50 mM $H_2O_2$ in water was investigated. Each film was freshly prepared on gold and the thickness was determined before and after the incubation from an AFM micrograph (Figure S7) obtained by carefully scratching the film with a plastic tip. The CV of $K_3[Fe(CN)_6]/K_4[Fe(CN)_6]$ was also recorded before and after the incubation. The relative change in thickness is shown in Figure 6 D. A dramatic change in thickness appears after only 24h incubation for p-NorEp and p-ALT films while for PDA a significant change is noticed only after 44h. Moreover, all the films show a remarkable decrease in the peak current when performing potassium ferro/ferri cyanide cyclic voltammetry, which was then completely recovered after degradation of the films, confirming a

complete removal of the film from the conductive surface as shown in Figure 6 E. Although polycatecholamine films have been shown to be highly stable in both aqueous and organic solvents[41], the observed degradation of the films in a relatively low concentration solution of $H_2O_2$ opens the possibility to selective degradation of films. This is an important property for the reduction of waste after end-of-life. In particular, at low concentrations, $H_2O_2$ is an environmentally-friendly oxidizer that can even be directly generated by some enzymes such as glucose oxidase, thereby providing a fully green process.

**Conclusions**

In this work the electrodeposition of two bioderived analogues of dopamine was successfully demonstrated and analyzed in detail. The preparation of the new ultrathin polymer film p-ALT, was accomplished for the first time using electropolymerization of the monomer 3-amino-L-tyrosine. The successful electrodeposition of the dopamine analogous norepinephrine was also reported in detail without pre-oxidation steps and the UV-visible spectra were recorded. The prepared films were well characterized chemically and physically using a combination of in-situ techniques, such as eQCM, spectroelectrochemistry and EIS, and standard techniques such as FTIR, AFM, and XPS. Comparisons to the well-known biopolymer PDA were also given. Not surprisingly, p-NorEp shares similar behavior with PDA both in the electrochemical preparation, with similar oxidation and reduction peaks, and in the quenching properties, a well-known characteristic for polycatecholamines. On the other hand, despite also being structurally similar to catecholamine, p-ALT presented different features such as non-limited deposition during the preparation at the electrode and a significant reduction in quenching capacity. These features together with the low impedance shown during the characterization highlight the possibility to use this polymer for the preparation of novel nanocomposite materials that might be difficult to achieve with other polycatecholamines due to their known stickiness and quenching properties. Possible applications could be the preparation of biosensing surfaces, where a low electrical resistance is desirable[60], or the embedding photoactive inorganic particles like quantum dots or nanorods for applications relying upon fluorescence or light interactions, for example sensors or photocatalysis. We also showed the complete degradation of the p-ALT films in mild conditions and this process could allow cradle-to-grave bioprocessing of these films. Further studies are warranted to determine the applicability of these films to enzyme triggered degradation pathways. In addition, the very smooth surface together with the possibility to finely control the thickness makes it

suitable for the preparation of biosensors *via* immobilization of DNA aptamers or peptides. The results presented here might set up a pathway for future green technologies based on the electrodeposition of polymeric films which might be prepared exploiting sunlight and degraded by enzymes.

AUTHOR INFORMATION

## Corresponding Author

* Sdharv@gmail.com, weil@mpip-mainz.mpg.de

.

## Author Contributions

Tommaso Marchesi D'Alvise and Dr. Sean Harvey prepared the samples, optimized the procedures, analyzed the data and wrote the manuscript. Sruthi Sunder and Julia Moser helped with the samples preparation. Roger Hasler performed the Optic fiber SPR experiments and Professor Dr. Wolfgang Knoll supervised and supported the SPR studies. Dr. Christopher Synatschke corrected the manuscript and helped with the scientific discussion throughout the project. Dr. Sean Harvey supervised the project. Professor Dr. Tanja Weil supported and supervised the whole project, helped with scientific discussion and with writing the manuscript. The manuscript was written through contributions of all authors. All authors have given approval to the final version of the manuscript.

## Funding Sources

Deutsche Forschungsgemeinschaft. Grant Number: 407426226

Marie Curie ITN BORGES. Grant Number: 813863

Max-Planck-Gesellschaft. Grant Number: Open Access Funding

# ACKNOWLEDGMENT

The authors acknowledge support by the Deutsche Forschungsgemeinschaft (DFG, German Research Foundation) under the Collaborative Research Center (CRC) Transregio 234 (No. 407426226, B04). This project has received funding from the European Union's Horizon 2020 research and innovation programme under the Marie Curie Skłodowska-Curie grant agreement No 813863 BORGES. Open Access funding provided by the Max Planck Society is acknowledged.

# ABBREVIATIONS

AFM, Atomic Force Microscopy; CV, cyclic Voltammetry; eQCM, electrochemical Quartz Crystal Microbalance; EIS, Electrochemical Impedance Spectroscopy; FTIR, Fourier Transform Infrared; p-ALT, poly-amino-L-tyrosine, PDA, polydopamine; p-NorEP, polynorepinephrine; XPS, X-ray photoelectron spectroscopy

# References


1 A. Gandini and T. M. Lacerda, *Prog. Polym. Sci.*, 2015, **48**, 1–39.

2 Y. Zhu, C. Romain and C. K. Williams, *Nature*, 2016, **540**, 354–362.

3 R. Mülhaupt, *Macromol. Chem. Phys.*, 2013, **214**, 159–174.

4 M. A. Rahim, S. L. Kristufek, S. Pan, J. J. Richardson and F. Caruso, *Angew. Chem. Int. Ed.*, 2019, **58**, 1904–1927.

5 T. S. Sileika, D. G. Barrett, R. Zhang, K. H. A. Lau and P. B. Messersmith, *Angew. Chem. Int. Ed.*, 2013, **52**, 10766–10770.

6 B. Lochab, S. Shukla and I. K. Varma, *RSC Adv.*, 2014, **4**, 21712–21752.

7 J.-J. Xu, X. Fang, C.-Y. Li, L. Yang and X.-Y. Chen, *aBIOTECH*, 2020, **1**, 97–105.

8 T. Fukuoka, Y. Tachibana, H. Tonami, H. Uyama and S. Kobayashi, *Biomacromolecules*, 2002, **3**, 768–774.

9 P. Salazar, M. Martín and J. L. González-Mora, *Polym. Sci. Res. Adv. Prat. Appl. Educ. Asp.*, 2007, **1**, 385–396.

10 S. Li, H. Wang, M. Young, F. Xu, G. Cheng and H. Cong, *Langmuir*, 2019, **35**, 1119–1125.

11 H. Lee, S. M. Dellatore, W. M. Miller and P. B. Messersmith, *Science,* 2007, **318**, 426–430.

12 D. Chen, Y. Mei, W. Hu and C. M. Li, *Talanta*, 2018, **182**, 470–475.

13 H. Zhang, J. Luo, S. Li, Y. Wei and Y. Wan, *Langmuir*, 2018, **34**, 2585–2594.

14 H. Guo, Z. Yao, J. Wang, Z. Yang, X. Ma and C. Y. Tang, *J. Memb. Sci.*, 2018, **551**, 234–242.

15 S. Daboss, J. Lin, M. Godejohann and C. Kranz, *Anal. Chem.*, 2020, **92**, 8404–8413.

16 B. Stöckle, D. Y. W. Ng, C. Meier, T. Paust, F. Bischoff, T. Diemant, R. J. Behm, K.-E. E. Gottschalk, U. Ziener and T. Weil, *Macromol. Symp.*, 2014, **346**, 73–81.

17 L. E. Aguilar, B. Tumurbaatar, A. Ghavaminejad, C. H. Park and C. S. Kim, *Sci. Rep.*, 2017, **7**, 9432.

18 S. Kim, L. K. Jang, H. S. Park and J. Y. Lee, *Sci. Rep.*, 2016, **6**, 30475.

19 V. Baldoneschi, P. Palladino, S. Scarano and M. Minunni, *Anal. Bioanal. Chem.*, 2020, **412**, 5945–5954.

20 G. Loget, J. B. Wood, K. Cho, A. R. Halpern and R. M. Corn, *Anal. Chem.*, 2013, **85**, 9991–9995.

21 J. H. Kim, M. Lee and C. B. Park, *Angew. Chem. Int. Ed.*, 2014, **53**, 6364–6368.

22 M. K. Sung, J. Rho, I. S. Choi, P. B. Messersmith and H. Lee, *J. Am. Chem. Soc.*, 2009, **131**, 2145–2156.

23 Y. Liu, X. Nan, W. Shi, X. Liu, Z. He, Y. Sun and D. Ge, *RSC Adv.*, 2019, **9**, 16439–16446.

24 S. Khetani, V. O. Kollath, E. Eastick, C. Debert, A. Sen, K. Karan and A. Sanati-Nezhad, *Biosens. Bioelectron.*, 2019, **145**, 111715.

25 F. Bernsmann, J. C. Voegel and V. Ball, *Electrochim. Acta*, 2011, **56**, 3914–3919.

26 J. Vatrál, R. Boča and W. Linert, *Monatsh. Chem.*, 2015, **146**, 1799–1805.

27 H. R. Gerding, C. Karreman, A. Daiber, J. Delp, D. Hammler, M. Mex, S. Schildknecht and M. Leist, *Redox Biol.*, 2019, **26**, 101251.

28 J. G. Bruno and J. L. Kiel, *Bioelectromagnetics*, 1994, **15**, 315–328.

29 M. Ambrico, P. F. Ambrico, A. Cardone, N. F. Della Vecchia, T. Ligonzo, S. R. Cicco, M. M. Talamo, A. Napolitano, V. Augelli, G. M. Farinola and M. D'Ischia, *J. Mater. Chem. C*, 2013, **1**, 1018–1028.

30 M. Garedew, C. H. Lam, L. Petitjean, S. Huang, B. Song, F. Lin, J. E. Jackson, C. M. Saffron and P. T. Anastas, *Green Chem.*, 2021, **23**, 2868–2899.

31 M. Bisaglia, S. Mammi and L. Bubacco, *J. Biol. Chem.*, 2007, **282**, 15597–15605.

32 S. Hong, J. Kim, Y. S. Na, J. Park, S. Kim, K. Singha, G. Il Im, D. K. Han, W. J. Kim and H. Lee, *Angew. Chem. Int. Ed.*, 2013, **52**, 9187–9191.

33 T. Marchesi D'Alvise, S. Harvey, L. Hueske, J. Szelwicka, L. Veith, T. P. J. Knowles, D. Kubiczek, C. Flaig, F. Port, K.-E. Gottschalk, F. Rosenau, B. Graczykowski, G. Fytas, F. S. Ruggeri, K. Wunderlich and T. Weil, *Adv. Funct. Mater.*, 2020, **30**, 2000378.

34 J. Pollet, F. Delport, K. P. F. Janssen, K. Jans, G. Maes, H. Pfeiffer, M. Wevers and J. Lammertyn, *Biosens. Bioelectron.*, 2009, **25**, 864–869.

35 I. Antohe, K. Schouteden, P. Goos, F. Delport, D. Spasic and J. Lammertyn, *Sensors Actuators, B Chem.*, 2016, **229**, 678–685.

36 A. T. Reiner, N. G. Ferrer, P. Venugopalan, R. C. Lai, S. K. Lim and J. Dostálek, *Analyst*, 2017, **142**, 3913–3921.

37 S. Kunimura, T. Ohsaka and N. Oyama, *Macromolecules*, 1988, **21**, 894–900.

38 A. Q. Zhang, C. Q. Cui, Y. Z. Chen and J. Y. Lee, *J. Electroanal. Chem.*, 1994, **373**, 115–121.

39 S. Mu, *Synth. Met.*, 2004, **143**, 259–268.

40 V. Ball, D. Del Frari, V. Toniazzo and D. Ruch, *J. Colloid Interface Sci.*, 2012, **386**, 366–372.

41 T. G. Barclay, H. M. Hegab, S. R. Clarke and M. Ginic-Markovic, *Adv. Mater. Interfaces*, 2017, **4**, 1601192.

42 L. Zhang and J. Lian, *J. Electroanal. Chem.*, 2007, **611**, 51–59.

43 M. Quinto and A. J. Bard, *J. Electroanal. Chem.*, 2001, **498**, 67–74.

44 N. Nishizawa, A. Kawamura, M. Kohri, Y. Nakamura and S. Fujii, *Polymers,* 2016, **8**, 62.

45 A. GhavamiNejad, L. E. Aguilar, R. B. Ambade, S. H. Lee, C. H. Park and C. S. Kim, *Colloids Interface Sci. Commun.*, 2015, **6**, 5–8.

46 M. B. Clark, J. A. Gardella, T. M. Schultz, D. G. Patil and L. Salvati, *Anal. Chem.*, 1990, **62**, 949–956.

47 J. W. Colson and W. R. Dichtel, *Nat. Chem.*, 2013, **5**, 453–465.

48 Y. Tokura, S. Harvey, C. Chen, Y. Wu, D. Y. W. Ng and T. Weil, *Angew. Chem. Int. Ed.*, 2018, **57**, 1587–1591.

49 O. Abou Mehrez, F. Dossier-Berne and B. Legube, *Chemosphere*, 2016, **145**, 464–469.

50 A. K. Dhara, K. Kumar, S. Kumari, U. P. Singh and K. Ghosh, *Transit. Met. Chem.*, 2020, **45**, 159–172.

51 S. Kunimura, T. Ohsaka and N. Oyama, *Macromolecules*, 1988, **21**, 894–900.

52 S. Mu, *Synth. Met.*, 2004, **143**, 259–268.

53 N. Singh, J. Nayak, K. Patel, S. K. Sahoo and R. Kumar, *Phys. Chem. Chem. Phys.*, 2018, **20**, 25812–25821.

54 P. Shi, X. Miao, H. Yao, S. Lin, B. Wei, J. Chen, X. Lin and Y. Tang, *Electrochim. Acta*, 2013, **92**, 341–348.

55 V. Ball, D. Del Frari, V. Toniazzo and D. Ruch, *J. Colloid Interface Sci.*, 2012, **386**, 366–372.

56 W. Qiang, W. Li, X. Li, X. Chen and D. Xu, *Chem. Sci.*, 2014, **5**, 3018–3024.

57 D. Chen, L. Zhao and W. Hu, *J. Colloid Interface Sci.*, 2016, **477**, 123–130.

58 D. Fan, X. Zhu, Q. Zhai, E. Wang and S. Dong, *Anal. Chem.*, 2016, **88**, 9158–9165.

59 P. Yang, S. Zhang, X. Chen, X. Liu, Z. Wang and Y. Li, *Mater. Horizons*, 2020, **7**, 746–761.

60 S. McGraw, E. Alocilja, A. Senecal and K. Senecal, *Biosensors*, 2012, **2**, 465–478.

61 S. A. Centeno and J. Shamir, *J. Mol. Struct.*, 2008, **873**, 149–159.